Formation of supramolecular clusters at the interface of zeolite X following the adsorption of rare-earth cations and their impact on the macroscopic properties of the zeolite.

Roberta Guzzinati, [a,b] Elena Sarti,[a] Martina Catani,[a] Valentina Costa,[a] Antonella Pagnoni,[a] Annalisa Martucci,[c] Elisa Rodeghero,[c] Donatella Capitani,[d] Massimiliana Pietrantonio,[e] Alberto Cavazzini, * [a] Luisa Pasti. *[a]

Abstract: The adsorption behavior of neodymium (Nd^{3+}) and yttrium (Y^{3+}) cations on synthetic FAU zeolite X in its sodium form (NaX) has been investigated by means of an approach based on both macroscopic (namely, adsorption isotherm determination and thermal analysis) and microscopic measurements (including solid-state NMR spectroscopy and X-ray powder diffraction). The multidisciplinary study has revealed some unexpected features. Firstly, adsorption constants of cations are not correlated to their ionic radii (or hydration enthalpy). The adsorption constant of Y^{3+} on NaX was indeed about twice that of Nd^{3+}, which is the opposite of what could be expected based on the size of the cations. In addition, adsorption was accompanied by partial dealumination of the zeolite framework. The extent of dealumination changed depending on exchanged cations. It was more significant on the Nd-exchanged zeolite than on the Y-exchanged one. The most interesting finding of this study, however, is the presence of supramolecular clusters composed of water, Nd^{3+}, residual sodium ions and extraframework aluminum at the interface of Nd-exchanged zeolite. The hypothesis that these host-guest complexes are responsible of the significantly different behavior exhibited by NaX towards the adsorption/desorption of Nd^{3+} and Y^{3+} has been formulated.

Introduction

Zeolites are natural or synthetic crystalline microporous materials comprised of basic unit TO_4 (where T is silicon, aluminum or other tetra-coordinated atoms). These units form 3-dimensional open porous structures made of channels and cages (or cavities) of discrete and specific size.[1] Based on the framework porosity, zeolites may be classified into small, medium, large and ultra-large structures. Pores are occupied by extraframework cations that counterbalance the negative charge resulting from the substitution of silicon by aluminum. Void spaces can also host water molecules, simple gases and larger molecules.[2]

Over the years, thanks to the great flexibility in their synthesis, zeolites of unique physico-chemical properties specifically designed to achieve superior performance in many fields of application,[3] such as molecular sieves,[4] heterogeneous catalysis,[5] adsorption and cation exchange [6] have been prepared. These materials are manufactured in a uniform phase-pure state that allows for careful tuning of both their pore architecture and chemical composition; in particular the silica-to-alumina ratio (SAR) that influences to a large extent the physico-chemical characteristics of zeolites. It is well known, indeed, that zeolites with high SAR are hydrophobic (largely employed, e.g., for adsorption of hydrophobic compounds) [7] while those with low SAR are intrinsically hydrophilic (widely used for the selective removal of cations from water through ionic exchange mechanism). [8]

Among the most interesting and versatile synthetic zeolites, those with FAU-type topology (i.e., NaX, NaY, Linde X, Ultrastable Y, all analogous to the natural zeolite Faujasite) consist of sodalite units (β-cage) linked together by double 6-rings (d6R) to give large cavities (referred also to as supercages or α-cages) accessible through a 12-ring window with diameter of around 6 Å (see Figure 1).

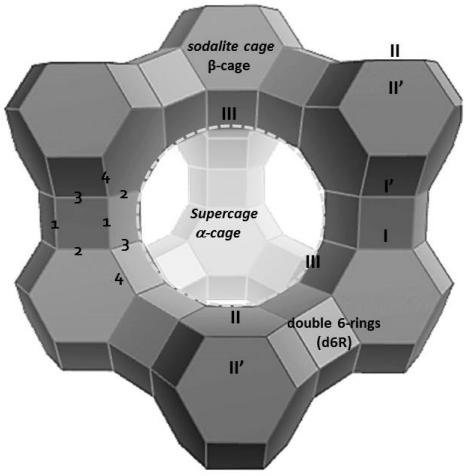

Figure 1. Structure of FAU-type zeolites viewed along [111]. Latin numbers indicate extra framework sites. Arabic ones are employed to label oxygen sites.

[a] Roberta Guzzinati, Elena Sarti, Valentina Costa, Luisa Pasti, Alberto Cavazzini, University of Ferrara, Department of Chemistry and Pharmaceutical Sciences, Via L. Borsari, 46,44121 Ferrara, Italy, E-mail: luisa.pasti@unife.it, alberto.cavazzini@unife.it.
[b] Roberta Guzzinati, Italian National Agency for New Technologies, Energy and Suitable Economic Development (ENEA), R. C. Bologna, Via Martiri di Monte Sole, 4, 40129, Bologna, Italy.
[c] Annalisa Martucci, Elisa Rodeghero, University of Ferrara, Department of Physics and Earth Sciences, Via Saragat, 1, 44121, Ferrara, Italy.
[d] Donatella Capitani, National Research Centre, Methodological Chemistry Institute CNR-IMC, Laboratory "Annalaura Segre", Via Salaria km 29, 300, 00015 Monterotondo (RM), Italy.
[e] Massimiliana Pierantonio, Italian National Agency for New Technology, Energy and Suitable Economic Development (ENEA) R. C. Casaccia, Via Anguillarese, 301, S. Maria di Galeria, Roma, Italy.

Supporting information for this article is given via a link at the end of the document.

Each supercage is interconnected to four others by windows of 7.4 Å diameter. [9] FAU-type zeolites are divided into X and Y classes, depending on their SAR. FAU zeolites X have SARs between 1 and 1.5. FAU zeolites Y, on the other hand, have SARs above 1.5. Zeolite X, in particular, is one of the most widely employed, aluminum-rich synthetic zeolite. The arrangement of exchangeable cations on the different crystallographic sites of this zeolite depends mainly on hydration/dehydration level, maximization of interactions with framework oxygen and, finally, minimization of electrostatic repulsions.

The type and localization of extraframework cations control and influence not only adsorption and ion exchange behavior of zeolites X but also their selectivity and catalytic activity. The fine control of these features has allowed for the development of engineered zeolites X employed in cutting-edge applications in heterogeneous catalysis [10] and in the developing of luminescent materials. [11] Sorption and cation exchange properties of zeolite X towards alkali metals, alkaline earth cations, transition metals, organic compounds and gases have been extensively investigated.[12] In contrast, there have been only a few reports on the use of NaX for the adsorption of rare-earth elements (REEs). Frising and al. reviewed the distribution of lanthanide cations in Faujasite, reporting that both lanthanum and cerium cations are located in different positions of NaX framework, including the center of the 12-ring window of the supercage, with the only exception of site III (see Figure 1). [13] More recently the location of lanthanum in an exchanged faujasite has been investigated by combining physicochemical measurements and DFT calculations. [14]

It is well known that partitioning of ions at the interface of zeolites and aqueous solutions is a very complex phenomenon involving the interplay of chemical, electrostatic (physical forces) and crystallographic factors, [15] the investigation of which can only be performed through a multidisciplinary study. Scope of this work is the investigation of the adsorption/desorption behavior of two trivalent rare-earth cations, neodymium (Nd^{3+}) and yttrium (Y^{3+}),[16] at the interface of sodium form of zeolite FAU X (usually denoted NaX). To this end, the information gathered from the interpretation of the adsorption isotherm of both cations on NaX [17] has been combined with that derived from the structural analysis of the zeolite before and after cation exchange. In particular, batch adsorption experiments at room temperature were employed to determine not only the mechanisms but also the kinetics of exchange process of Nd^{3+} and Y^{3+} with NaX. On the other hand, Rietveld refinements of X-ray powder diffraction (XRPD) [18] and magic angle spinning (MAS) NMR spectroscopy [19], performed before and after the exchange process, allowed to estimate the distribution of extraframework REE cations in the zeolite framework following adsorption. They have also permitted to evidence some relevant structural modifications of the zeolite framework. In particular for Nd-exchanged zeolite, not only dealumination has been observed but also formation of supramolecular clusters on the surface of zeolite has been experimentally demonstrated.

In zeolite dealumination, aluminium atoms are removed from the framework. They form octahedrally coordinated extraframework structures. These phenomena have been already observed in zeolites exposed to steam and hot water. [20] Recently, it has been reported that also adsorption of REEs (depending on the characteristics of exchanged cations) can lead to irreversible dealumination of zeolite. [21] DFT calculations on zeolite X exchanged with lanthanum indicated hydroxylated La^{3+} cations interacting with the sodalite cage via OH groups as the possible model of dealumination. [14]

On the other hand, to the best of our knowledge, this study is the first report showing the evidence of formation of supramolecular clusters at the interface of NaX zeolite. Additionally, these clusters are more complex both in structure and composition than those hypothesized on the basis of DFT calculation. [14] Whether these structural changes may impact on the macroscopic properties of zeolites is something that requires further investigation. The point could be particularly important, for instance, to explain the improved performance of some exchanged-zeolites in heterogeneous catalysis [10] as well as the use of these materials in optical devices. [11] We attempted to correlate the presence of host-guest complexes to the remarkably different behavior of Nd- or Y-exchanged zeolites in terms of cation exchange reversibility. Desorption studies performed at different temperature have indeed shown significant differences in the recovery of Y^{3+} and Nd^{3+} from REEs exchanged NaX. As a whole, the information gathered by this study can also be relevant to the evaluation of NaX as cation exchange material for REE cations. In recent years, the research into new techniques for the selective recovery of REEs from different matrixes has attracted much attention, due to the increasing demand–supply gap of REEs.[22] Cation exchange can represent an eco-friendly, cost-effective alternative to conventional methods employed for extraction/recovery of REEs, such as, e.g., solvent extraction, and selective oxidation/reduction. [23]

Results and Discussion

Cation exchange of metal ions from aqueous solutions depends strongly on pH. At excessively high pHs, hydroxyl ions may complex and/or precipitate metal cations from aqueous solutions. On the other hand, when pH becomes excessively acidic ($pH < 3$), either reduction of the cation exchange capacity of the zeolite due to protonation of its binding sites, or degradation of the zeolite may occur.[24] Thus, at the beginning of this work the minimum pH needed to start precipitation of Nd^{3+} and Y^{3+} was experimentally investigated. It was found that at pH slightly greater than 6, precipitation of hydroxy-complexes of Nd^{3+} and Y^{3+} begins. Therefore, the adsorption capacity of zeolite NaX towards Nd^{3+} and Y^{3+} was evaluated in a series of adsorption batch experiments in a pH range from 3.5 to 5.5. In all cases, pH was measured at the end of batch experiments to account for the hydrolytic activity of the zeolite.[25] Cation exchange experiments were conducted at constant room temperature and contact time (100 min). For both cations, the cation exchange capacity was found to be essentially constant regardless of pH (see Figure S1 of Supporting Information). Thus, following this

preliminary information, all data measured in this work refer to the intermediate pH of 4.5. Figure S2 of Supporting Information, reporting the results of cation exchange experiments performed at different contact times (10 min - 24 h), shows that 100 min is long enough to reach equilibrium. The cation exchange kinetics was investigated in a series of experiments in which the uptake was measured at different contact times. Data were fitted by means of a pseudo-second-order (PSO) model. The pseudo-second-order rate expression has been widely applied to the adsorption of organic pollutants from aqueous solutions, as well as to investigate cation exchange processes. [6] This model was able accurately to describe the experimental data, as demonstrated by the high determination coefficient (R^2 > 0.99) obtained for both cations (details under Supporting Information) indicating that cation exchange seems to be the rate-controlling step of the adsorption process.

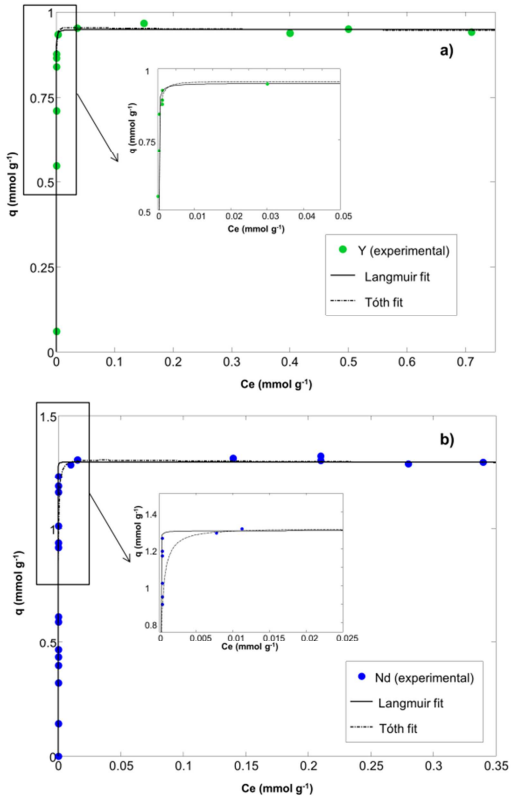

Figure 2 a, b: Adsorption isotherms of yttrium^{3+} (a) and neodymium^{3+} (b) on X.

Figure 2 shows the cation exchange isotherms of Y^{3+} (Figure 2a) and Nd^{3+} (Figure 2b) with Na^+ of zeolite NaX, measured through batch experiments at room temperature. As can be seen from this figure, cation exchange isotherms of both cations exhibit a pronounced concave curvature. The isotherms are characterized by a very steep initial zone that quickly reaches a plateau concentration (saturation zone). Therefore, from a thermodynamic viewpoint, cation exchange of both rare-earth cations on X in its sodium form is strongly favorable.[26] This information, together with the relatively fast adsorption kinetics exhibited by Nd^{3+} and Y^{3+} (see before), shows that NaX is a promising cation exchange material for rare-earth cations.

To investigate the cation exchange mechanisms of Nd^{3+} and Y^{3+} on zeolite FAU NaX at room temperature, the experimental data were fitted to different adsorption isotherm models [27], namely the Langmuir and Tóth isotherms [28] (see Table 1). These adsorption isotherms (see Table 1). These isotherms describe two inherently different adsorption mechanisms. The Langmuir model indeed represents ideal adsorption in ion exchange reactions on a homogenous surface. This means that the model does not account for interactions between exchanged cations, nor for ion exchanged-solvent interactions.[29] Following this model, each zeolite cage is thus considered as an independent site, or subsystem, able to exchange only one cation at a time. In addition, all sites are energetically equivalent. The Langmuir model is possibly excessively simple to describe the real complexity of interactions at the interface of zeolite NaX. Nevertheless, it has been the widely employed to model adsorption and cation exchange data on different kinds of zeolites exhibiting the behavior of Figure 2. Essentially, the assumption is made that the energies of all the possible interactions are close enough that they can be averaged, so a single energy and a single affinity constant can be defined, which characterize all the exchangeable sites on the surface. The Tóth isotherm, on the other hand, accounts for an asymmetrical quasi-Gaussian energy distribution function of the cation exchange sites. Thus, it describes adsorption on a heterogeneous surface, where most of the exchangeable sites have an energy lower than the mean value.[30] The so-called heterogeneity parameter *t* appearing in the Tóth isotherm (see Table 1) varies between 0 and 1. It is correlated to the width of the energy distribution function. The smaller the value of *t*, the larger the width of the distribution and, therefore, the more heterogeneous the surface.[28] For $t = 1$, the Tóth isotherm corresponds to the Langmuir one. In Figure 2, the best-interpolating Langmuir and Tóth isotherms are represented by continuous-red and dotted-blue lines, respectively. In Table 1, the results of nonlinear fitting analysis are reported (errors on the parameters are given at the 95% confidence interval).

As can be seen, not only from the coefficient of determination listed in this table (in all cases R^2>0.98), but also by inspection of Figure 2, both the Langmuir and the Tóth models allow a very accurate fit of experimental data. In particular, in the case of Y^{3+} (Figure 2a), the best-interpolating Langmuir and Tóth isotherms cannot basically be distinguished from each other. On the other hand, some minimal differences can be observed between the two models in the inset of Figure 2b, where the Langmuir isotherm seems to match slightly better the curvature of Nd^{3+} isotherm compared to the Tóth one. The analysis of data reported in Table 1 confirms that, from a statistical viewpoint, there is no difference between the Langmuir and Tóth models. Indeed, the heterogeneity parameter for both cations is, at 95% of probability, not significantly different from 1. Therefore, the Tóth model converges to the single-site Langmuir model. Accordingly, cation exchange experiments show that cations of a given element react on sites of zeolite that are energetically

equivalent to each other.[31] However, this information cannot be used either to assess which positon of the framework is involved in the cation exchange process, or to understand whether both cations are exchanged on the same site (but with different energies) or on different positions of the framework (*vide infra*). The cation exchange capacity of Nd^{3+} was some 30% higher (1.3 mmol per gram of zeolite) than that of Y^{3+} (9.5×10^{-1} mol g^{-1}).

Table 1. Cation exchange isotherm parameters. q_e (mmol g^{-1}): exchanged concentration at equilibrium; C_e (mmol dm^{-3}): concentration in the solution at equilibrium; K_L, K_T (dm^3 $mmol^{-1}$): affinity constants for the Langmuir and the Tóth models, respectively; q_s (mmol g^{-1}) cation exchange capacity; *t* heterogeneity parameter in the Tóth model (see text for further details). Confidence bounds at 95% of probability are reported in parenthesis.

Model	Parameters	Nd^{3+}	Y^{3+}
Langmuir			
	q_s	1.32	9.52×10^{-1}
$q_e = \frac{q_s K_L C_e}{1+K_L C_e}$	(mmol g^{-1})	(1.26–1.37)	($9.22–9.83\times10^{-1}$)
	K_L	10.38×10^{2}	22.53×10^{2}
	(dm^3 $mmol^{-1}$)	($7.58–13.17\times10^{2}$)	($16.72–28.44\times10^{2}$)
	R^2	0.9893	0.9849
Tóth			
	q_s	1.30	9.48×10^{-1}
	(mmol g^{-1})	(1.26–1.35)	($9.24–9.73\times10^{-1}$)
$q_e = \frac{q_s K_T C_e}{\left[1+(K_T C_e)^t\right]^{1/t}}$	K_T	6.43×10^{2}	12.42×10^{2}
	(dm^3 $mmol^{-1}$)	($4.58–8.27\times10^{2}$)	($2.57–22.32\times10^{2}$)
		2.233	1.306
	t	(0.9306, 3.535)	(0.7486, 1.863)
	R^2	0.9936	0.9891

Differences between saturation capacities indicate that fractions of Na sites in NaX exchanged either with Y or Nd are different from each other's. In contrast, the affinity constant of Y^{3+} (22.5×10^{2} dm^3 $mmol^{-1}$) was found to be larger (+115%) than that of Nd^{3+} (10.4×10^{2} dm^3 $mmol^{-1}$). This remarkable difference in affinity between the two cations is difficult to explain. The common understanding, indeed, is that affinity of a given cation towards a zeolite depends on some specific properties, such as, basically, the hydration and ionic radius of the cation, its hydration enthalpy and solubility. The enthalpy of hydration (ΔH_{hyd}) increases in absolute value with the inverse of the ionic radius. The ionic radius decreases across the series of REEs. Y^{3+}, which is considered a heavy REE, has a smaller ionic radius than does Nd^{3+}, a member of the light REEs. Its enthalpy of hydration is higher in absolute value ($\Delta H_{hyd,Y3+} = -3583$ kJ mol^{-1}) than that of Nd^{3+} ($\Delta H_{hyd,Nd3+} = -3403$ kJ mol^{-1}). [32] Therefore, one should expect the affinity constant of Y^{3+} on the zeolite to be smaller than that of Nd^{3+}.[33] Data in Table 1, however, have shown an opposite trend, demonstrating that thermodynamic considerations based only on hydration enthalpy cannot explain the experimental evidence. One hypothesis could be the presence on NaX of different sites able to preferentially exchange Na with Y and or Nd respectively. On one hand, these findings are consistent with the observations by Gładysz-Płaska et al. on the exchange process of lanthanides in zeolite Y.[34] They report that, for these compounds, the inverse dependence of the affinity constant on the ionic radius is not strictly followed or only scarcely accurate. To explain the different exchange energies of lanthanides on zeolite Y, these authors considered the different stabilization of cations in the framework. Following their explanation, it is the capability of cations to coordinate simultaneously extra-framework water molecules and framework oxygen atoms that mainly determines the degree of stabilization in the given surroundings. More recently it has been pointed out that our understanding of bonding phenomena to different hydroxyl groups on a mineral surface is still far from complete and, more specifically, that the true nature of lanthanide interactions with minerals/oxides is definitely understudied. [35]

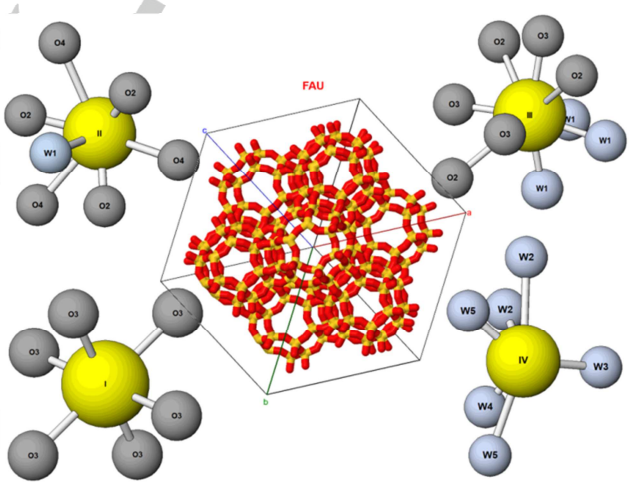

Figure 3. Location of framework atoms and water molecules in NaX.

With the aim of further investigating these challenging aspects on zeolite X, a structural investigation was carried out. The goal of this study was to gain insights into the microscopic features of the adsorption process, such as the localization of cation adsorption sites in the zeolite framework, and their occupancy.

The structural analysis by XRPD started with the investigation of NaX (see Figure 3).

Zeolite X belongs to the *Fd-3* space group. In its sodium form, Na^+ cations were found to be distributed among four different crystallographic sites (see Figure 3), in agreement with what was found also on zeolite X. [36] Na^+ is bonded to six framework oxygens ($6\times$O3) in site I, to six O atoms and one water molecule ($3\times$O2, $3\times$O4, $1\times$W1) in site II, to six O atoms and three water molecules ($3\times$O2, $3\times$O3, $3\times$W1) in site III, whereas to only six water molecules in site IV (W2, W3, $2\times$W4 and $2\times$W5), (see Figure 3). Crystallographic details are given

as Crystallographic Information Framework (CIF) files (see also Table S3-S5 in Supplementary Information). The mean values of the tetrahedral T1–O and T2–O bond lengths are 1.646 and 1.718 Å, respectively. The measured T–O–T mean angle is 137.7°. The difference between the smallest (132.7°) and the largest (142.3°) T–O–T angles indicates a distortion of the framework. On the basis of the refined occupancy and symmetry, 91 Na^+ cations were found in the structure of NaX, in very good agreement with the maximum number theoretically achievable per unit cell (p.u.c.). As far as the water content is concerned, five extraframework sites were detected, hosting about 265 molecules p.u.c. They correspond to roughly 25% of the zeolite dry weight (dw), in excellent agreement with the weight loss estimated in the 100–900 °C range by thermogravimetric analysis (about 24.8% zeolite dw, see Figure 4).

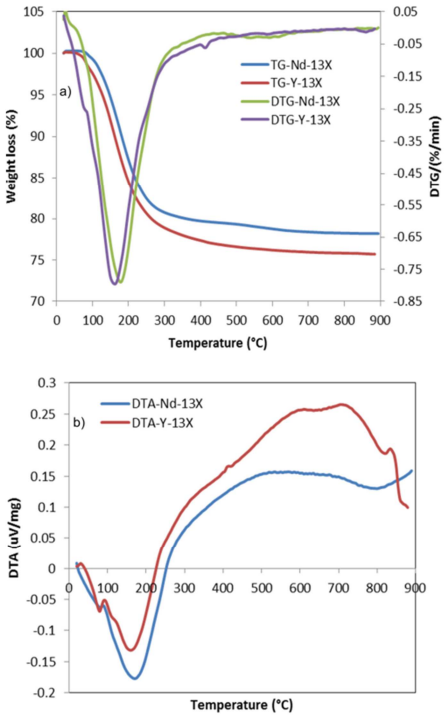

Figure 4 a,b: a) Thermogravimetry (TG) of [Na, Nd]-X (blue line) and [Na, Y]-X (red line), and derivative thermogravimetry (DTG) curves of [Na, Nd]-X (green line) and [Na, Y]-X (violet line), b) Differential thermal analysis (DTA) of [Na, Nd]-X (blue line) and [Na, Y]-X (red line)

After Y^{3+} and Nd^{3+} exchange, strong variations in the XRPD patterns were observed. In addition, a partial loss of crystallinity was observed in the Nd-exchanged sample (*vide infra*). However, based on these measurements, no significant symmetry changes could be observed for any exchanged zeolite (see Figure 5). Consequently, the same *Fd-3* space group, already employed for NaX, was adopted for the refinement of both Y- and Nd-X structures. By carefully inspecting Figure 5, the occurrence of new diffraction peaks can be observed in the pattern of Nd-exchanged zeolite. Noticeably, these signals are not present in the diffractogram of Y-exchanged zeolite. It has already been reported in the literature for zeolite Y that, after adsorption of rare-earth cations, variations in the unit cell parameters can occur due to partial hydrolysis of the framework. [37] Similar evidence has now been observed in Nd-exchanged zeolite X. In this case, the acidity of the aqueous complex of Nd^{3+} can be invoked to explain variations in the XRD pattern and thus in the unit cell parameters. This hypothesis has been validated also by NMR spectra, as will be discussed later on. Difference Fourier maps allow recognition of a maximum centered at 0.0429(1) 0.0429(1) 0.0429(1) three-fold coordinated to O3 framework oxygen, which can be assigned to an extraframework Al ion (Al1-O3 × 3 = 2.227(6) Å).

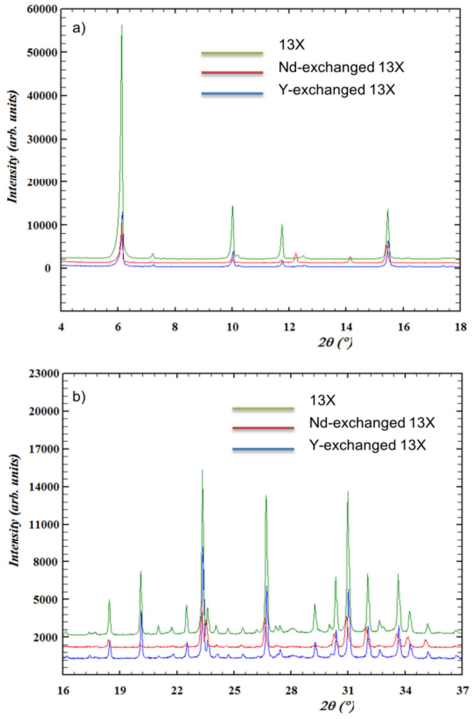

Figure 5 a,b: XRPD diffraction patterns of Na-X (green line), [Na, Nd]-X (red line) and [Na, Y]-X (blue line) a) low 2θ angles b) middle 2θ angles.

The improved fit between observed and calculated diffraction patterns before (Figure 6a) and after (Figure 6b) the detection of extraframework Al cations confirmed the correctness of the refined structure model. The [Na, Nd]-X final error indices for the 6409 reflections were R_{wp}=12.26% and 9.62%, R_p=9.57% and 7.70% , $R_F^2(2219_{obs})$= 15.36% and 10.02% before and after Al extraframework detection, respectively (where $R_p = \Sigma[Y_{io} - Y_{ic}]/\Sigma Y_{io}$; $R_{wp} = [\Sigma wi(Y_{io} - Y_{ic})^2/\Sigma wi Y_{io}^2]^{0.5}$; $R_F^2 = \Sigma|F_o^2 - F_c^2|/|F_o^2|$). In both samples the Rietveld refinement reveals that the REE ion exchange is not complete: Y^{3+} and Nd^{3+} ions occupy just one position at the center of the hexagonal window between the sodalite cage and the supercage (site II).

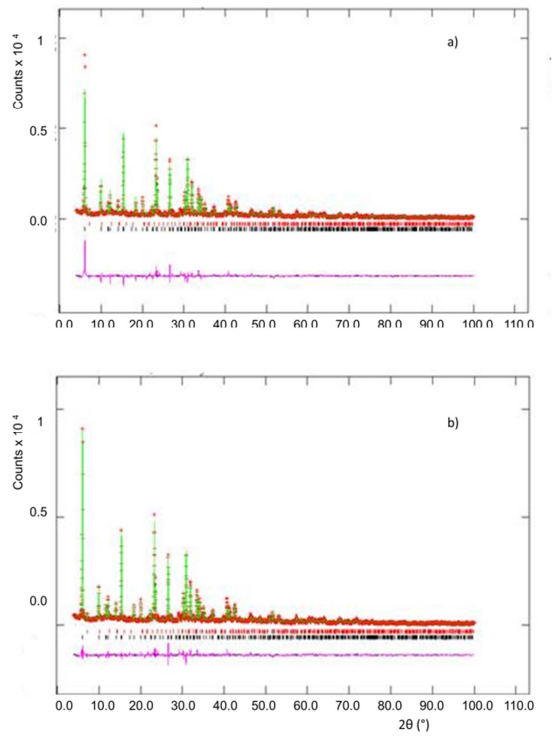

Figure 6 a,b: Observed (crosses), calculated (continuous line), and difference curve (bottom line) resulting from the Nd-exchanged sample before (a) and after (b) the detection of extraframework Al cations.

Their relative occupancy (25% and 45% for Y and Nd, respectively) gives rise to a rare-earth cation content of 8.6 and 13.6 cations p.u.c. for Y^{3+} and Nd^{3+}, respectively (see Figure 7). These values correspond to about 7% and 12% w/w for Y^{3+} and Nd^{3+} respectively, and agree well with the cation exchange capacities of NaX obtained from cation exchange isotherms.

In the following, for sake of brevity, the NaX partially exchanged with Nd and Y is indicated as [Na, Nd]X and [Na,Y]X respectively. Additionally, the Rietveld refinement indicated variations in the unit cell parameters of exchanged zeolites in comparison to NaX. Indeed, in [Na,Y]X the crystallographic axis *a* is 24.9747(3) Å (the number in parenthesis is the error as single standard deviation of the last digit) and the cell volume is 15577.7(4) $Å^3$ (R_{wp}= 9.82%, R_p= 8.30% , $R_F^2(1846_{obs})$= 10.32%). The value of *a* becomes 25.0143(4) Å (cell volume = 15651.8(4) $Å^3$) in [Na,Nd]X. Finally, in NaX *a* is 24.9859(3) Å and the cell volume is 15598.7(3) $Å^3$. The variations of cell volume of partially exchanged zeolites with respect to NaX suggest the incorporation of REEs in the zeolite pore structure. After cation exchange with Na^+ in NaX, indeed, both Nd^{3+} and Y^{3+} ions approach O4 framework oxygens.

This process is accompanied by a variation in the opening of the zeolite framework pore system and, consequently, in the crystallographic free areas. Sodium ions not substituted by REE ions in the exchanged zeolites occupy sites Na1 (corresponding to III, see Figure 1) and Na2 (corresponding to IV, see Figure 1), respectively. Contrary to that observed for NaX, sodium ions were not detected in the center of the hexagonal prism (site I) of both [Na,Nd]X and [Na,Y]X. In fact, the short distances between sodium cations in site III and extraframework Al sites (1.1980(8) Å) prevent their simultaneous occupancy of neodymium site I in exchanged zeolite.

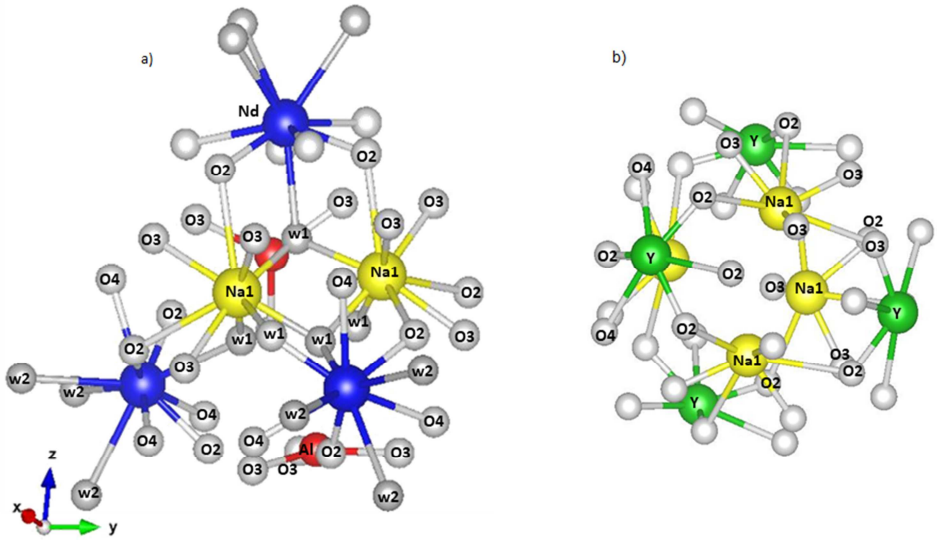

Figure 7 a,b: Coordination of sodium (yellow spheres), extraframework aluminium (red spheres), neodymium (blue spheres), yttrium (green spheres) cations in (a) [Na,Nd]X and (b) [Na,Y]X. Oxygens of the framework and water molecules are represented as gray spheres.

The coordinates of the oxygen atoms of extraframework water molecules were found by the difference electron density map after Rietveld refinement. A total of 240 and 248 water molecules p.u.c. for [Na,Y]X and [Na,Nd]X, respectively, were estimated.

They correspond approximately to an average value of 24% of zeolite dw, in very good agreement with the weight losses observed by thermogravimetric analysis (about 22% and 24% zeolite dw for [Na,Nd]X and [Na,Y]X respectively, see Figure 4). More interestingly, water molecules act as bridge between sodium cations in site III and Nd ions in [Na,Nd]X, contributing to a cluster formation involving extraframework Al mediated by water molecules (W1), whose structure is shown in Figure 7a. These findings are consistent with previous reports on the dealumination of zeolites occurring after cation exchange with REE ions. [14] The presence of similar clusters was not detected in [Na,Y]X; very interestingly the W1 site was now empty.

To further investigate the possible dealumination of zeolite NaX after exchange of Nd^{3+} with Na^{+}, a series of solid-state ^{29}Si and ^{27}Al MAS NMR measurements were performed. Through solid state NMR, it is in principle possible to distinguish Si and Al atoms with different coordination states. In particular, Al atoms occupying lattice positions in the zeolite framework are tetrahedrally coordinated. On the other hand, those that occupy interstitial positions in the framework (i.e., extra-framework Al) are octahedrally coordinated.[38]

^{29}Si MAS NMR spectra were obtained under experimental conditions which ensured the data to be quantitatively reliable. Spectra of NaX, [Na,Y]X and [Na,Nd]X zeolites are reported in Figure 8 a, b, and c, respectively. The occurrence of aluminum atoms in the second coordination sphere of the silicon to which they are bonded through oxygen atoms produces a systematic change in the ^{29}Si chemical shifts.[39] Specifically, the spectrum of NaX showed five well-defined resonances at −84.5, −89.1, −93.9, −98.4, and −102.7 ppm that were assigned to silicon having 4, 3, 2, 1 and 0 aluminum atoms in the second coordination sphere, respectively. These resonances were labeled with Si(4Al), Si(3Al), Si(2Al), Si(1Al), and Si (0Al) (see Figure 8a). The spectrum was deconvoluted to obtain the peak areas (Table 2). Peak areas were used to calculate the Si/Al ratio of the zeolite framework:

$$\frac{Si}{Al} = \frac{\sum_{n=0}^{4} I(nAl)}{\sum_{n=0}^{4} 0.25 n I(nAl)} = 1.26$$

The low Si/Al ratio of 1.26 ± 0.03 indicated that the Si(4Al) peak was very dominant in the ^{29}Si spectrum.

After exchange with Y^{3+}, the ^{29}Si spectrum of [Na,Y]X again showed five well-observable resonances, which were deconvoluted to obtain the parameters reported in Table 2. After the exchange, the Si/Al ratio turned out to be the same as that before the exchange, namely 1.28 ± 0.03. Similar values of Si/Al were also found by analyzing the composition of solutions after acidic dissolution of zeolites (see Table S2 in Supplementary Information). However, the exchange with Y^{3+} induced a line-broadening and a chemical shift of 2 ppm in the Si(0Al) resonance, and about 1 ppm in the Si(4Al) and Si(2Al) resonances, whereas Si(3Al) and Si(1Al) were unaffected (Figure 8b).

In contrast, in [Na,Nd]X the ^{29}Si spectrum broadened markedly, impairing the observation of distinct resonances, and preventing any spectral deconvolution (Figure 8c). However, it can be qualitatively noticed that the exchange with Nd^{3+} induced a change in the signals at -105 ppm and -81 ppm, which can be related to dealumination and to the presence of SiOH defects, respectively.

The ^{27}Al spectra of NaX, [Na,Y]X and [Na,Nd]X are reported in Figure 8 d, e, and f. The zeolite NaX showed an almost symmetrical peak at about 61.5 ppm, assigned to tetrahedrally coordinated framework aluminum; see Figure 8d. After the exchange with Y^{3+}, the peak of tetrahedrally coordinated Al broadened slightly and shifted to 59 ppm, and a very weak peak ascribable to octahedrally coordinated aluminum appeared at about 2 ppm. Again, after the exchange with Nd^{3+}, the peak of the tetrahedrally coordinated Al broadened slightly. However, it retained a rather symmetrical shape. A broad and weak peak of octahedrally coordinated aluminum appeared at about 2 ppm. The amount of octahedrally coordinated aluminum was found to be higher in [Na,Nd]X than in [Na,Y]X.

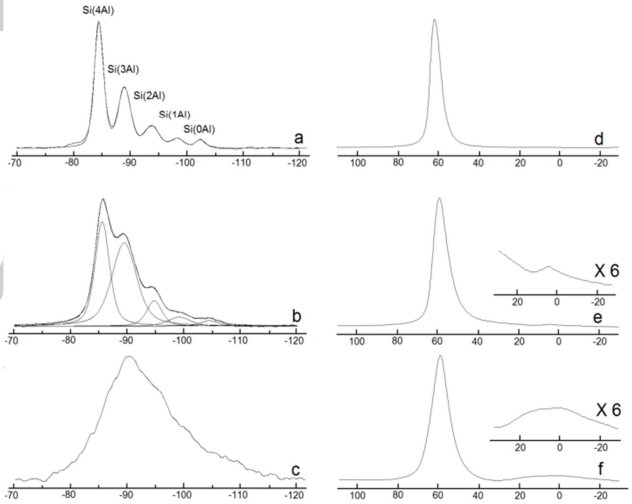

Figure 8 a,b,c,d,e,f: ^{29}Si MAS NMR spectra of (a) zeolite X, (b) zeolite X after exchange with Y, and (c) zeolite X after exchange with Nd. ^{27}Al MAS NMR spectra of (d) X zeolite, (e) X after exchange with Y, and (f) zeolite X after exchange with Nd. In the inserts the region of octahedrally coordinated aluminum is shown with a vertical multiplication of ×6.

In the last part of this study, the desorption behavior of [Na,Nd]X and [Na,Y]X was investigated in a series of desorption experiments performed at different temperature (up to 70°C, see Supporting Information for more information) by using NH_4Cl (3 mol L^{-1}) aqueous solution at pH 4.5 as regeneration agent. Surprisingly, the behavior of the two

exchanged zeolites was significantly different. It was found that at room temperature, recovery of Y^{3+} was almost quantitative while that of Nd^{3+} was smaller than 80% (details are given in Supporting Information). Even by increasing temperature (desorption experiments were performed up to 70°C), Nd^{3+} recovery did not improve significantly (see Figure S3 of Supporting Information). This observation might correlate to the presence of previously described host–guest interactions involving Nd^{3+} ions.

Table 2. Parameters obtained by deconvoluting ^{29}Si MAS spectra of zeolite X before and after the exchange with Y

Peak	Before exchange with Y		After exchange with Y	
Si(nAl)	ppm	I(nAl) (%)	ppm	I(nAl) (%)
Si(4Al)	–84.5	48.73	–85.5	37.83
Si(3Al)	–89.1	31.06	–89.3	47.83
Si(2Al)	–93.9	12.35	–94.7	9.20
Si(1Al)	–98.4	4.61	–98.6	4.84
Si(0Al)	–102.7	3.26	–104.7	2.3

Conclusions

The multidisciplinary study on NaX zeolite exchanged with trivalent cations Nd^{3+} and Y^{3+} presented in this work has revealed that, from a molecular viewpoint, the exchange behavior of the two cations presents very different features. These findings confirm that exchange of rare earth cations with sodium in zeolite X is a very complex process, which strongly depends on the considered ion. Not surprisingly, the traditional paradigm employed to explain cation exchange properties of zeolite (essentially based on the ionic radius of cations) was unable to predict what was experimentally observed in this work. Superficial supramolecular structures involving Nd^{3+} but not Y^{3+} were evidenced and deeply characterized by structural analysis based on XRPD and solid-state NMR. The presence of these structures was correlated to the different macroscopic behavior of NaX towards the exchange properties of the two cations. Perhaps more interestingly, it will be to investigate whether supramolecular-like structures could be involved in the optical properties or in the catalytic activity of metal-doped zeolites. Last but not least, this work also suggests that, thanks to its high saturation capacity, fast cation exchange kinetics and high recovery, NaX can be efficiently used for purification and recovery of rare earth cations through adsorption or adsorption-like processes.

Experimental Section

Material and Characterization Technique. Chemicals used for all batch experiments were of analytical grade; details are reported in Supplementary Information. Zeolite NaX (purchased by Tosoh) was dried at 200 °C for 3h before batch experiments. (see Supplementary Information).

Cation exchange capacity was determined by using single-cation aqueous solutions of Nd^{3+} and Y^{3+}, at different initial concentrations (5, 10, 20, 50, 70, 100, 150 and 200 mg L^{-1} for both cations), placed in contact with zeolite with a solid/liquid ratio of 1:1. The solutions were kept at 25 °C under stirring during the contact time. Different pH values (3.5; 4.5; 5.5) were tested to investigate the effect of pH on the cation exchange efficiency. pH was modified with NaOH 10 N. All batch experiments were carried out in duplicate. Nd^{3+} and Y^{3+} in sample solutions, before and after batch processes, were quantified by ICP-OES (Perkin-Elmer Optima 3100 XL) (axial view) equipped with a solid-state charge-coupled device detector (CCD), a peristaltic pump and a low-flow GemCone nebulizer coupled to a cyclonic spray chamber. Background correction was carried out using a two-points method. Analytical lines of Y 324.227 and 371.029 nm, and Nd 401.225 nm were selected for quantitative determination. The amount of exchanged cations at equilibrium, qe (mg g^{-1}), was calculated from the mass balance equation:

$$q_e = (C_i - C_e)\frac{V}{M}$$

where *Ci* and *Ce* (mg L^{-1}) are the liquid-phase concentrations of Nd and Y at initial time and at equilibrium respectively; *V* (L) is the volume of the solution and *M* (g) is the mass of dry zeolite used. Na13-X and samples of saturated zeolite exchanged with Nd and Y (i.e. Na,Nd]X and [Na,Y]X) were used for NMR and structural investigations. [Na,Nd]X and [Na,Y]X samples were ion-exchanged using aqueous solution of Nd^{3+} and Y^{3+} respectively at 298 K for 24 h, filtered, and then washed with water. The ion-exchanged zeolite was then dried at 383 K overnight.

Zeolite composition was determined by ICP-OES (emission wavelengths: 288.16 and 237.34 nm for Si and Al, respectively). 0.5 g of samples were mineralized by microwave acid digestion (HNO_3, HF and H_3BO_3) at 200 °C and high pressure (200 psig), with 20 min dwell time.

Thermal analyses. Thermogravimetric (TG) and differential thermal analysis (DTA) measurements of the REE- exchanged zeolites were performed in air using an STA 409 PC LUXX®-Netzch operating at 10 °C min^{-1} heating rate, from room temperature (RT) to 900 °C.

X-ray powder diffraction measurements and structure determination. X-ray powder diffraction (XRPD) patterns of zeolites before and after yttrium and neodymium exchange were measured on a Bruker D8 Advance Diffractometer equipped with a Si (Li) solid-state detector, (Cu Kα1,2 radiation, 3–110° 2θ range, counting time of 12 s per 0.02° 2θ step). The structural refinements were performed using the Rietveld method with the GSAS-EXPGUI software packages. The starting coordinates for the cations and bound water were obtained from difference Fourier maps. Framework and extraframework atomic coordinates, and temperature factors for NaX, [Na,Nd]X and [Na,Y]X respectively, are provided in Tables S3-S5 in Supplementary Information (SI). The background curve was fitted by a Chebyshev polynomial with 14 coefficients. The shape of the diffraction peak was modeled with a pseudo-Voigt function with three Gaussian and two Lorentzian line-broadening terms.

Solid-state NMR

Samples were finely ground, inserted in 4 mm zirconia rotors, and sealed with Kel-F caps. Spectra were recorded on a Bruker Avance III NMR spectrometer operating at the ^{1}H frequency of 400.13 MHz. ^{29}Si MAS NMR spectra were recorded at 79.49 MHz, with spin rate 8 KHz. The p/2 pulse width was 3 ms, and the recycle delay was optimized to 60 s. Spectra were acquired with a time domain of 1024 data points and Fourier transformed using 2048 data points. The ppm scale was externally referenced to tetramethylsilane. ^{27}Al MAS NMR spectra were recorded at 104.26 MHz, with spin rate 10 KHz. The p/2 pulse width was 1.5 ms, and the recycle delay was optimized to 5 s. Spectra were acquired with a time domain of 512 data points and Fourier transformed using 1024 data points. The ppm scale was externally referenced to aluminum nitrate. ^{29}Si MAS spectra were deconvoluted by using the dm2011 software package.

Acknowledgements

Authors acknowledge dr. Ercolina Bianchini of the University of Ferrara (Ferrara, Italy) and Giorgia N. Torelli of Arpa-Lazio (Rome, Italy) for technical support.

Keywords: zeolites • Rare Earths • exchange interactions • adsorption • supramolecular clusters

[1] C. Baerlocher, L. B. McCusker, D. H. Olson, *Atlas of zeolite framework types*, 6th edn, Elsevier, **2007**.

[2] P. Demontis, H. Jobic, M. A. Gonzalez, G. B. Suffritti, *J. Phys. Chem. C* **2009**, *113*, 12373-12379.

[3] a) C. Wang, J. Li, X. Sun, L. Wang, X. Sun, *J. Environ. Sci.* **2009**, *21*, 127-136; b) A. Corma, *J. Catal.* **2003**, *216*, 298-312; c) M. E. Davis, *Nature* **2002**, *417*, 813-821; d) J. D. Sherman, *Proc. Natl. Acad. Sci. USA* **1999**, *96*, 3471-3478.

[4] M. E. Davis, R. F. Lobo, *Chem. Mater.* **1992**, *4*, 756-768.

[5] a) T. Yokoi, H. Mochizuki, S. Namba, J. N. Kondo, T. Tatsumi, *J. Phys. Chem. C* **2015**, *119*, 15303-15315; b) V. Komvokis, L. X. L. Tan, M. Clough, S. S. Pan, B. Yilmaz, in *Zeolites in Sustainable Chemistry*, Springer, **2016**, pp. 271-297; c) S. Andrejkovičová, A. Sudagar, J. Rocha, C. Patinha, W. Hajjaji, E. F. da Silva, A. Velosa, F. Rocha, *Appl. Clay Sci.* **2016**, *126*, 141-152.

[6] a) H. Ghasemi Mobtaker, H. Kazemian, M. A. Namdar, A. Malekinejad, M. R. Pakzad, *Iran. J. Chem. Chem. Eng.* **2008**, *27*, 111-117; b) L. Pasti, E. Rodeghero, E. Sarti, V. Bosi, A. Cavazzini, R. Bagatin, A. Martucci, *RSC Adv.* **2016**, *6*, 54544-54552; c) S. Malamis, E. Katsou, *J. Hazard. Mater.* **2013**, *252-253*, 428-461; d) M. D. Oleksiak, A. Ghorbanpour, M. T. Conato, B. P. McGrail, L. C. Grabow, R. K. Motkuri, J. D. Rimer, Chem. Eur. J. 2016, 22, 15957-16324.

[7] a) A. Martucci, L. Pasti, M. Nassi, A. Alberti, R. Arletti, R. Bagatin, R. Vignola, R. Sticca, *Micropor. Mesopor. Mat.* **2012**, *151*, 358-367; b) L. Pasti, E. Sarti, A. Cavazzini, N. Marchetti, F. Dondi, A. Martucci, *J. Sep. Sci.* **2013**, *36*, 1604-1611.

[8] a) L. Ćurković, Š. Cerjan-Stefanović, T. Filipan, *Water Res.* **1997**, *31*, 1379-1382; b) P. Hadi, C. Ning, J. D. Kubicki, K. Mueller, J. W. Fagan, Z. Luo, L. Weng, G. McKay, *Inorg. Chem. Front.* **2016**, *3*, 502-513; c) K. S. Hui, C. Y. H. Chao, S. C. Kot, *J. Hazard. Mater.* **2005**, *127*, 89-101.

[9] G. Maurin, P. Llewellyn, T. Poyet, B. Kuchta, *J. Phys. Chem. B* **2005**, *109*, 125-129.

[10] a) R. J. Davis, *J. Catal.* **2003**, *216*, 396-405. b) K. M. Jinka, J. Sebastian, R. V. Jasra, *J. Mol. Catal. A: Chem.* **2007**, *274*, 33-41.

[11] a) H. Maas, A. Currao, G. Calzaferri, *Angew. Chem. Int. Ed.* **2002**, *41*, 2495–2497. b) S. Chakraborty, M. Severance, T. Young, P. K. Dutta, *J. Phys. Chem. C* **2015**, *119 (27)*, 15491-15499.

[12] a) V. K. Jha, M. Nagae, M. Matsuda, M. Miyake, *J. Environ. Manage.* **2009**, *90*, 2507-2514; b) M. Jeffroy, A. Boutin, A. H. Fuch, *J. Phys. Chem. B* **2011**, *115*, 15059-15066; c) O. O. Ltaief, S. Siffert, S. Fourmentin, M. Benzina, *C. R. Chim.* **2015**, *18*, 1123-1133; d) C. Covarrubias, R. Arriagada, J. Yáñez, R. García, M. Angélica, S. D. Barros, P. Arroyo, E. F. Sousa-Aguiar, *J. Chem. Technol. Biotechnol.* **2005**, *80*, 899-908.

[13] a) T. Frising, P. Leflaive, *Micropor. Mesopor. Mat.* **2008**, *114*, 27-63. b) J.V. Smith, J.M. Bennett, E.M. Flanigen, *Nature* **1967**, *215*, 241-244. c) D.H. Olson, G.T. Kokotailo, J.F. Charnell, *J. Coll. Interf. Sci*, **1968**, *28*, 305-314. d) D.S. Shy, S.H. Chen, J. Lievens, S.B. Liu, K.J. Chao, *J. Chem. Soc., Faraday Trans.* **1991**, *87*, 2855-2859. e) H.S. Park, K. Seff, *J. Phys. Chem. B* **2000**, *104*, 2224-2236. f) D.H. Olson, G.T. Kokotailo, J.F. Charnell, *Nature* **1967**, *215*, 270-271. g) F.D. Hunter, J. Scherzer. *J. Catal.* **1971**, *20*, 246-259.

[14] F. Schüßler, E. A. Pidko, R. Kolvenbach, C. Sievers, E. J. M. Hensen, R. A. van Santen, J. A.; Lercher, *J. Phys. Chem. C* **2011**, *115*, 21763-21776.

[15] Mitchell, S., Milina, M., Verel, R., Hernández-Rodríguez, M., Pinar, A. B., McCusker, L. B. and Pérez-Ramírez, J. *Chem. Eur. J.* **2015**, *21*, 14156–14164.

[16] a) Z. Chen, *J. Rare Earths* **2011**, *29*, 1-6; b) P. Thyssen, K. Binnemans, in *Handbook on the Physics and Chemistry of Rare Earths, Vol. 41*, Elsevier, **2011**, pp. 1-93.

[17] a) P. F. Zito, A. Caravella, A. Brunetti, E. Drioli, G. Barbieri, *J. Chem. Eng. Data* **2015**, *60*, 2858-2868; b) O. Bortolini, A. Cavazzini, P. P. Giovannini, R. Greco, N. Marchetti, A. Massi, L. Pasti, *Chem. Eur. J.* **2013**, 19, 7802-7808

[18] a) C. E. A. Kirschhock, B. Hunger, J. Martens, P. A. Jacobs, *J. Phys. Chem. B* **2000**, *104*, 439-448; b) E. Rodeghero, A. Martucci, G. Cruciani, E. Sarti, A. Cavazzini, V. Costa, R. Bagatin, L. Pasti, *J. Phys. Chem. C* **2017**, *121*, 17958-17968; c) P. Cao, O. Khorev, A. Devaux, L. Sägesser, A. Kunzmann, A. Ecker, R. Häner, D. Brühwiler, G. Calzaferri, P. Belser, *Chem. Eur. J.* **2016**, *22*, 4046-4060.

[19] a) H. Ernst, D. Freude, H. Pfeifer, I. Wolf, *Stud. Surf. Sci. Catal.* **1994**, *84*, 381-385; b) G. Engelhardt, in *Stud. Surf. Sci. Catal., Vol. 137*, Elsevier Science B.V, **2001**, pp. 387-417; c) E. Lippmaa, M. Maegi, A. Samoson, M. Tarmak, G. Engelhardt, *J. Am. Chem. Soc.* **1981**, *103*, 4992-4996; d) L. Gueudré, A. A. Quoineaud, G. Pirngruber, P. Leflaive, *J. Phys. Chem. C* **2008**, *112*, 10899-10908; e) M. Feuerstein, M. Hunger, G. Engelhardt, J. P. Amoureux, *Solid State Nucl. Magn. Reson.* **1996**, *7*, 95-103.

[20] a) S. Prodinger, H. Shi, S. Eckstein, J. Z. Hu, M. V. Olarte, D. M. Camaioni, J. A. Lercher, *Chem. Mater.* **2017**, *29*, 7255-7262. b) S. Prodinger, M. A. Derewinski, A. Vjunov, S. D. Burton, I. Arslan, J. A. Lercher, *J. Amer. Chem. Soc.* **2016**, *138(13)*, 4408-4415.

[21] C. Deng, J. Zhang, L. Dong, M. Huang, L. Bin, G. Jin, J. Gao, F. Zhang, M. Fan, L. Zhang, Y. Gong, *Sci. Rep.* **2016**, *6*, 23382.

[22] a) D. Dupont, K. Binnemans, *Green Chem.* **2015**, *17*, 856-868; b) J. Yang, T. Retegan, B. M. Steenari, C. Ekberg, *Sep. Purif. Technol.* **2016**, *166*, 117-124; c) C. J. Ferron, P. Henry, *Can. Metall. Q.* **2015**, *54*, 388-394; d) K. Binnemans, P. T. Jones, B. Blanpain, T. Van Gerven, Y. Yang, A. Walton, M. Buchert, *Journal of Cleaner Production* **2013**, *51*, 1-22.

[23] a) F. Xie, T. A. Zhang, D. Dreisinger, F. Doyle, *Miner. Eng.* **2014**, *56*, 10-28.b) L. V. Resende, C. A. Morais, *Miner. Eng.* **2010**, *23*, 277-280.

[22] a) M. W. Munthali, M. A. Elsheikh, E. Johan, N. Matsue, *Molecules* **2014**, *19*, 20468-20481; b) A. Petushkov, J. Freeman, S. C. Larsen, *Langmuir* **2010**, *26*, 6695-6701; c) G. J. Kramer, R. A. Van Santen, *J. Am. Chem. Soc.* **1993**, *115*, 2887-2897.

[23] a) R. Harjula, J. Lehto, J. H. Pothuis, A. Dyer, R. P. Townsend, *J. Chem. Soc., Faraday Trans.* **1993**, *89*, 971-976; b) K. Margeta, A.

Farkas, M. Šiljeg, N. Z. Logar, *Natural Zeolites in Water Treatment-How Effective is Their Use - Chap.5*, INTECH Open Access Publisher, **2013**.

[24] M. D. LeVan, G. Carta, C. M. Yon, *Perry's Chemical Engineers' Handbook: Adsorption and Ion Exchange*, McGraw-Hill, **1997**.

[25] J. Rouquerol, F. Rouquerol, P. Llewellyn, G. Maurin, K. S. W. Sing, *Adsorption by powders and porous solids: principles, methodology and applications (2nd edition)*, Academic press, **2013**.

[26] F. Rouquerol, I. Rouquerol, K. Sing, Adsorption by Powders and Porous Solids-Principles Methodology and Applications, Academic Press, London, **1999.**

[27] G. Guiochon, A. Felinger, D. G. G. Shirazi, *Fundamentals of preparative and nonlinear chromatography*, Academic Press, **2006**.

[28] a) A. Cavazzini, K. Kaczmarski, P. Szabelski, D. Zhou, X. Liu, G. Guiochon, *Anal. Chem.* **2001**, *73*, 5704-5715; b) L. Pasti, N. Marchetti, R. Guzzinati, M. Catani, V. Bosi, F. Dondi, A. Sepsey, A. Felinger, A. Cavazzini, *TrAC*, **2016**, 81, 63-68.

[29] S. H. Chen, K. J. Chao, T. Y. Lee, *Ind. Eng. Chem. Res.* **1990**, *29*, 2020-2023.

[30] S. Cotton, *Lanthanide and actinide chemistry*, John Wiley & Sons, **2013**.

[31] a) D. W. Smith, *J. Chem. Educ* **1977**, *54*, 540; b) S. L. Bertha, G. R. Choppin, *Inorg. Chem.* **1969**, *8*, 613-617.

[32] A. Gładysz-Płaska, M. Majdan, S. Pikus, W. Lewandowski, *J. Colloid Interface Sci.* **2007**, *313*, 97-107.

[33] A. Gładysz-Płaska, M. Majdan, S. Pikus, *J. Colloid Interface Sci.* **2008**, 317, 409-423.

[34] Y. I. Smolin, Y. F. Shepelev, I. K. Butikova, S. P. Zhdanov, N. N. Samulevich, *Kristallografiya* **1979**, *24*, 461-468.

[35] a) J. G. Nery, M. V. Giotto, Y. P. Mascarenhas, D. Cardoso, F. M. Z. Zotin, E. F. Sousa-Aguiar, *Microporous Mesoporous Mater.* **2000**, *41*, 281-293; b) M. Czjzek, H. Fuess, T. Vogt, *J. Phys. Chem.* **1991**, *95*, 5255-5261; c) A. K. Cheetham, M. M. Eddy, J. M. Thomas, *J. Chem. Soc., Chem. Commun.* **1984**, 1337-1338; d) E. F. T. Lee, L. V. C. Rees, *Zeolites* **1987**, *7*, 446-450; e) E. F. T. Lee, L. V. C. Rees, *Zeolites* **1987**, *7*, 143-147.

[36] C. A. Fyfe, G. C. Gobbi, J. S. Hartman, J. Klinowski, J. M. Thomas, *J. Phys. Chem.* **1982**, *86*, 1247-1250.

[37] K. J. D. MacKenzie, M. E. Smith, *Multinuclear solid-state nuclear magnetic resonance of inorganic materials, Vol. 6*, Elsevier, **2002**.

Entry for the Table of Contents (Please choose one layout)

Layout 1:

FULL PAPER

The adsorption of rare-earth elements (REEs) on hydrophilic zeolites have been investigated. The information gathered from both macroscopic and microscopic techniques reveal that dealumination occur during cation exchange process. The extraframework aluminum with water, Nd^{3+} and residual sodium ions form a supramolecular clusters on the surface of Nd-exchanged zeolite.

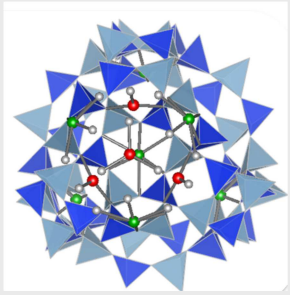

*Author(s), Corresponding Author(s)**

Page No. – Page No.

Title

Layout 2:

FULL PAPER

((Insert TOC Graphic here; max. width: 11.5 cm; max. height: 2.5 cm))

*Author(s), Corresponding Author(s)**

Page No. – Page No.

Title